Conditional existence of Donnan potential in soft particles and surfaces: Dependence on steric effects mediated by electrolyte ions and structural charges

Nicolas Lesniewska, Audrey Beaussart, Jérôme F.L. Duval

Conditional existence of Donnan potential in soft particles and surfaces: dependence on steric effects mediated by electrolyte ions and structural charges.

Nicolas Lesniewska*, Audrey Beaussart, Jérôme F.L. Duval*

Université de Lorraine, CNRS, Laboratoire Interdisciplinaire des Environnements Continentaux (LIEC), UMR 7360, Vandoeuvre-lès-Nancy F-54500, France

*Corresponding authors: nicolas.lesniewska@univ-lorraine.fr, jerome.duval@univ-lorraine.fr

Graphical Abstract

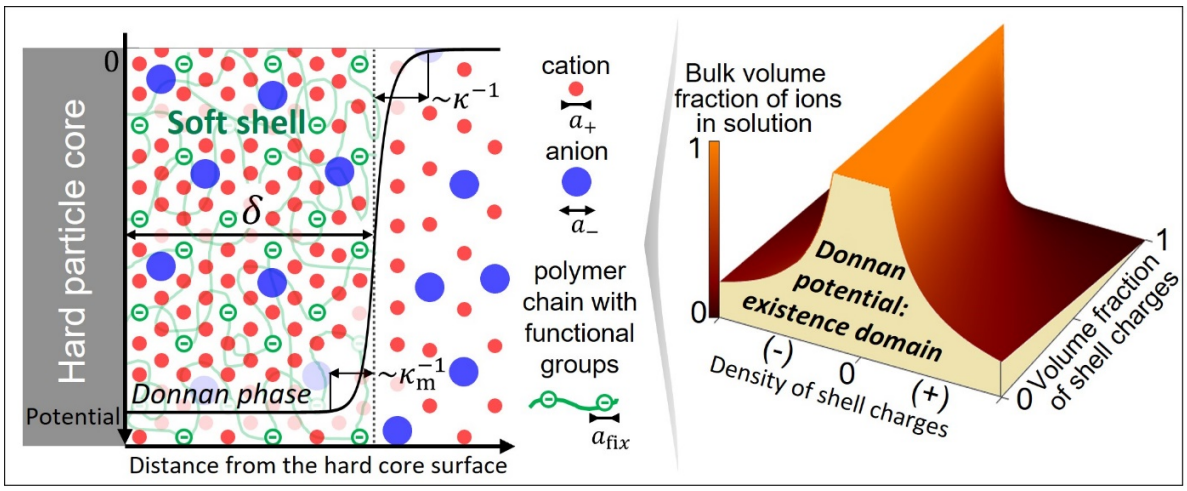

Abstract.

When a charged layer decorating a particle or a macroscopic surface is equilibrated with an electrolyte solution, a constant Donnan potential is established through that layer due to charge-driven accumulation of counterions and companion exclusion of coions. This situation arises when the thickness of the surface layer well exceeds the screening Debye length, a condition derived from mean-field Poisson-Boltzmann theory within point-like charge approximation. Herein, we revisit this condition underlying the applicability of Donnan electrostatic representation with the account of steric effects mediated by the sizes of the electrolyte ions and structural layer charges. A transcendental equation is derived for the Donnan potential as a function of sizes and valences of anions and cations, electrolyte concentration and size of the layer charges, and a closed-form expression is provided for symmetrical electrolytes. Therefrom we evidence that the existence of a Donnan potential is conditioned not only to large values of the layer thickness compared to a here-defined Debye length operative within the shell, but to additional verification of a criterion that involves space charge density of the layer, solution ionic strength and electrolyte nondiluteness parameter. Illustrative computational examples show how the existence and magnitude of the Donnan potential depend on the key molecular descriptors of the electrolyte and soft interface, and they further quantify the deviations from predictions based on classical Donnan potential expression valid for dilute electrolytes.

Keywords: Soft particles/interfaces, Electrostatics, Donnan potential, Steric effects, Modified Poisson-Boltzmann theory

1. Introduction.

Electrostatics plays a key role in the reactivity of particles and (bio)interfaces, e.g. colloid stability [1], ion adsorption [2], electrokinetics [3], polyelectrolyte swelling [4], cell biology [5-7], or blue energy harvesting [8]. Accordingly, modelling the electrostatics of charged interfaces and particles is of paramount importance, and formalisms reported for that purpose include the well-known mean-field Poisson-Boltzmann (PB) theory [9] and extensions thereof [10-22], and advanced molecular simulations [2,23-27]. Electrostatics of so-called soft colloids, i.e. colloids that consist partly or entirely of ion-permeable polyelectrolyte-like material with 3D distributed structural charges (e.g. microbial surfaces, viruses, engineered particle surface coatings, natural organic matter, macromolecules) [3,28-32], has received much attention by the community due to the ubiquity of these colloidal systems in biological and environmental settings [31,32], and their use in applications as diverse as drug delivery [33], degradation of organic pollutants [34], water treatment [35] or control of pathogens biofilm formation [36].

Following the pioneering work by Ohshima on soft surface electrostatics (cf. [3,29] and references therein), the equilibrium potential distribution at the interface formed between an electrolyte solution and a hard (ion-impermeable) core-soft shell particle, a porous particle (i.e. devoid of core) or a polyelectrolyte-coated planar surface has been derived from numerical and analytical solutions of PB equation with account of the charge contributions from both the electrolyte ions and the functional groups distributed within the shell material [29-32,37-40]. Solutions of PB equation have been further reported for soft particles in homo- or hetero-electrostatic interaction configurations [41-43] and for heterogeneous soft surface layers defined by a density of structural charges that varies with space [39,44]. A case of practical interest naturally emerges from the PB equation written for a soft surface layer whose thickness exceeds significantly the screening Debye length (hereafter denoted as $1/\kappa$): this is the Donnan situation where the electrostatic potential is constant inside the charged layer and decays to zero value over distances of the order $1/\kappa$ on both sides of the soft layer/electrolyte solution interface [45-48]. Under such a condition, Ohshima [45] demonstrated the equivalence between PB-derived expression of the interfacial potential drop – the so-called Donnan potential – and the one reported earlier by assuming simple local electroneutrality within the layer [49,50]. Remarkably, it is only recently that a direct support of Donnan potential theory was evidenced by tender-ambient pressure X-ray photoelectron spectroscopy measurements on ion-exchange membranes equilibrated with electrolyte solutions [51], while earlier indirect measurements have been reported on charged hydrogels by in-situ microelectrode voltammetry [52]. The Donnan partitioning of ions at charged surfaces and permselective interfaces has major implications in biology, as e.g. it affects the permeability of the membrane of Gram-negative bacteria to

nutrients or antibiotics [7], it contributes to bacterial survival under adverse (osmotic) environments [53] and it connects to biological functions like electric signalling in nervous system [54].

Whereas Donnan potential is achieved in charged surface layers at sufficiently high salt concentrations where the condition of thin electric double layer (EDL) compared to soft surface layer thickness is met, the combined effects of ion size *and* size of layer charges on interfacial Donnan partitioning of ions have – to the best of our knowledge – received little attention, despite the expected increase of the contributions of such effects with increasing electrolyte concentration [55-57]. A modification of the mean-field PB equation for soft interfaces and corresponding derivation of Donnan potential expression, have been reported so far for the only restrictive case of symmetrical electrolytes where anions and cations are assumed to have similar size, and considering layer charges as point-like [58-60]. Under these conditions, Lesniewska et al. [60] further derived an expression underlying the applicability of the Donnan representation for soft surface layer electrostatics as a function of the nondiluteness of the electrolyte, thereby evidencing that the condition of a sufficiently thin electric double layer is not sufficient to warrant the development of a Donnan potential in a charged soft surface layer.

Here, we further elaborate on this latest development and report an original expression for the Donnan potential in the most generic situation where anions and cations are defined by dissimilar valences and sizes, and where the size of charges carried by the soft surface layer is considered explicitly. This extension calls for the exploitation of an involved expression for the mixture entropy of the {layer charges/ions} system and of the corresponding PB formulation, as derived recently by Lesniewska et al. [60]. In turn, the formalism leads to a rationale of the situations where a Donnan potential cannot develop in the surface layer, even at high salt concentrations, due to limitation in the neutralization of layer charges by ions as a result of excluded volumes of anions, cations and functional groups carried by the layer. Illustrative computations further quantify the effects of electrolyte concentration, size/valence of ions and layer charges on *both* the existence domain and magnitude of the Donnan potential, while evidencing the moderate to severe misevaluation of the Donnan potential by predictions applicable to dilute systems where steric effects are discarded. Among the important results provided in this work is the derivation of the expression for the thickness of the electric double layer operative inside the charged surface layer, as a function of the ions- and shell charges- properties that govern steric effects.

2. Theory.

2.1. Electrostatics of soft interfaces.

In this section, we recall the basics of the electrostatic formalism recently developed by Lesniewska et al. [60] for soft interfaces in aqueous media. We elaborate below on this formalism with the objective to formulate explicitly the conditions underlying the existence of a Donnan potential in a given shell layer depending on the nondiluteness of the electrolyte. Herein, we consider a spherical core-shell particle with radius $r_\mathrm{p} = r_\mathrm{c} + \delta$, where r_c (m) and δ (m) are the particle core radius and shell layer thickness, respectively (**Figure 1**). The developments below hold in the electric double layer regime $\kappa r_\mathrm{p} \gg 1$ where $1/\kappa$ (m) is the Debye layer thickness defined by $1/\kappa = 1/\sqrt{2F^2 I/(RT\varepsilon_0\varepsilon_\mathrm{s})}$ with ε_0 the dielectric permittivity of the vacuum, ε_s the relative dielectric permittivity of the aqueous medium, R the gas constant, T the absolute temperature, F the Faraday number, and I (mol m^{-3}) the solution ionic strength. Adopting a radial coordinate system where $r = 0$ refers to the centre of the particle, we introduce for convenience the dimensionless radial position X defined by $X = \kappa(r - r_\mathrm{c})$. In the following, we further consider an electrolyte solution with cations and anions of *unsigned valences* z_+ and z_-, and *effective* radii a_+ (m) and a_- (m), respectively, with a_+^3 and a_-^3 their volumes assumed incompressible. The (number) densities of the cations and anions at radial position r are denoted as $c_{+,-}(r)$ (m^{-3}), and their bulk concentrations are defined by $c_{+,-}(r \to \infty) = c_{+,-}^\infty$ with the electroneutrality condition given by $z_+ c_+^\infty - z_- c_-^\infty = 0$ (autoprotolysis of water is neglected). The latter condition is systematically verified upon introduction of the number density c_0 (m^{-3}) defined by $c_0 = c_+^\infty / z_- = c_-^\infty / z_+$. In turn, solution ionic strength I is provided by $I = z_+ z_- (z_+ + z_-) c_0 / (2N_\mathrm{A})$ where N_A is the Avogadro number.

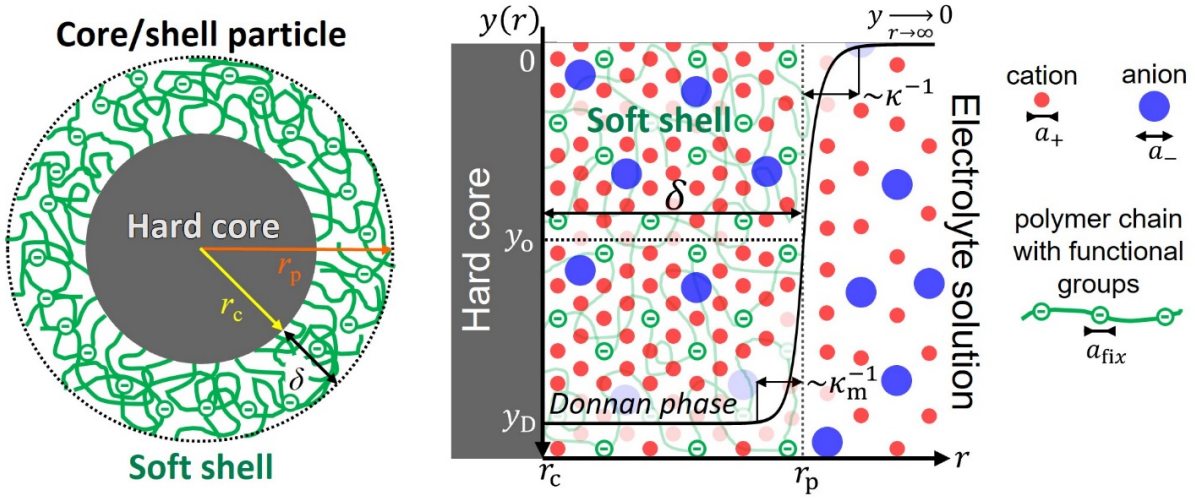

Figure 1. (Left) Schematic representation of a core-polyelectrolyte shell particle where the nomenclature adopted for the radial coordinate system (r), the particle core radius (r_c) and the shell thickness (δ) is specified. (Right) Zoom of the core/shell/aqueous electrolyte interfaces for cases where a Donnan potential is achieved in the particle shell layer. In the current work, the finite size of cations and anions $(a_{+,-})$ and that of the shell charges (a_{fix}) carried by the polymer chains constituting the shell layer are considered for the formulation of the electrostatic potential distribution within and outside the shell layer. In the shown example, the surface of the particle core is uncharged so that the electric field at $r = r_c$ is zero, and the particle shell is negatively charged. The purpose of the work is to formulate explicitly the conditions validating such a Donnan electrostatic situation depending on the geometric descriptors of the particle, the nondiluteness of the electrolyte, the excluded volume and density of the charges distributed within the shell component of the core-shell particle. $1/\kappa_m$ and $1/\kappa$ refer to the thickness of the screening Debye layers operative in the shell medium and in the outer electrolyte solution, respectively. $y(r)$, y_o and y_D correspond to the (dimensionless) potential at position r, the potential at the outer surface of the shell layer and the Donnan potential, respectively. Cf. details in the text.

In the developments below, we denote as a_{fix} (m) the radius of the structural charges (incompressible volume a_{fix}^3) distributed within the particle shell layer. To ease developments, and in line with common assumptions [3,29,42,43], the distribution of the structural charges within the shell is considered homogeneous so that the shell charge density denoted as $\rho_{fix}(r)$ (C m^{-3}) is given by

$$\rho_{fix}(r) = \begin{cases} \rho_0 & \text{for } r_c \le r \le r_p \\ 0 & \text{for } r > r_p \end{cases} \quad (1)$$

where $|\rho_0| = Zec_{fix,0}$ is the density of shell charges with unsigned valence Z and number density $c_{fix,0}$ (m^{-3}), and e is the elementary charge. Similarly, we introduce $c_{fix}(r) = |\rho_{fix}(r)|/(Ze)$ (m^{-3}) the number density of shell charges at position r. In the electric double layer regime defined by $\kappa r_p \gg 1$, the mean-

field Poisson-Boltzmann equation applicable to soft interfaces (termed **SMFPB** equation) and modified to account for the steric effects mediated by the size of the electrolyte ions and shell charges, reads [60]

$$\frac{\mathrm{d}^2 y(X)}{\mathrm{d}X^2} = \frac{n_-(X) - n_+(X)}{z_+ + z_-} - \frac{\rho_{\mathrm{fix}}(X)}{2IF} \tag{2}$$

where $\psi(r)$ (V) is the electrostatic potential at position r and $y(r) = F\psi(r)/RT$ is the dimensionless potential. Within the framework of this study, Eq. (2) does not involve the terms formulated by Lesniewska et al. [60] that originate from ion-ion correlations and dielectric decrement effect because their respective contributions were shown to be irrelevant for the cases of interest here where Donnan electrostatic representation is applicable [60]. The quantities $n_+(r) = c_+(r)/c_+^\infty$ and $n_-(r) = c_-(r)/c_-^\infty$ in Eq. (2) correspond to the (dimensionless) concentrations of cations and anions at position r, respectively. Discarding ion-ion correlations and dielectric effect, $n_{+,-}(r)$ are defined by (for $a_+ \geq a_-$)

$$\begin{cases} n_+(r) = \dfrac{\mathrm{e}^{-z_+ y(r)}}{g_{\mathrm{cc}}(y(r))} & \text{(a)} \\ n_-(r) = \dfrac{f_{\mathrm{cc}}(y(r))\mathrm{e}^{z_- y(r)}}{g_{\mathrm{cc}}(y(r))} & \text{(b)} \end{cases} \tag{3}$$

where f_{cc} and g_{cc} are functions of the potential distribution $y(r)$ defined by

$$\begin{cases} f_{\mathrm{cc}}(y(r)) = \left(\dfrac{1 - \nu + a_-^3 c_0 z_+ \mathrm{e}^{z_- y(r)}}{1 - a_+^3 c_0 z_-} \right)^{(a_+/a_-)^3 - 1} & \text{(a)} \\ g_{\mathrm{cc}}(y(r)) = \dfrac{f_{\mathrm{cc}}(y(r))(1-\nu) + a_+^3 c_0 z_- \mathrm{e}^{-z_+ y(r)} + a_-^3 c_0 z_+ f_{\mathrm{cc}}(y(r))\mathrm{e}^{z_- y(r)}}{1 - a_{\mathrm{fix}}^3 c_{\mathrm{fix}}(r)} & \text{(b)} \end{cases} \tag{4}$$

with $\nu = \sum_{\mathrm{ion}\, i} a_i^3 c_i^\infty$ (<1) a measure of the nondiluteness of the electrolyte. This definition of ν, adopted here for a convenient formulation of the Donnan electrostatic potential (cf. developments below), differs from the one adopted in [60] and originally defined on the basis of geometric arguments by Kilic et al. [61]. Eqs. (3)-(4) hold for $a_+ \geq a_-$, and equivalent formulation for $a_- \geq a_+$ is obtained by interchanging the terms $\mathrm{e}^{z_- y}$ and $\mathrm{e}^{-z_+ y}$ and the subscripts '+' and '-' in Eqs. (3)-(4). In Eq. (4), the function $g_{\mathrm{cc}}(y(r))$ accounts for the decrease in ion concentrations at position r due to excluded volume effects, as compared to the common mean-field situation where ions and shell charges are point-like [21,60]. In addition, $f_{\mathrm{cc}}(y(r))$ in Eq. (4) reflects the way in which an asymmetry in anion and cation sizes impacts on the potential distribution $y(r)$, with the limit $f_{\mathrm{cc}}(y(r)) = 1$ achieved for $a_+ = a_-$.

2.2. Donnan potential: the classical picture of point-like charges.

For core-shell particles featuring a shell density distribution given by Eq. (1), the Donnan phase (when existing) corresponds to the shell region where the electrostatic field is zero (**Figure 1**). This situation is achieved for soft particulate (and planar) interfaces whose shell dimension well exceeds the thickness of the electrical double layer thickness $1/\kappa$. The corresponding condition $\kappa\delta \gg 1$ thus applies to sufficiently thick shell layers and/or sufficiently high electrolyte concentrations [45]. Under such conditions, Ohshima formulated the potential distribution within the shell layer and at the shell solution interface [62]. He evidenced that the Debye layer thickness operative at the shell side of the interface, denoted as $1/\kappa_{\mathrm{m}}$ (m), generally differs from the conventional Debye screening length $1/\kappa$ according to

$$1/\kappa_{\mathrm{m}} = 1/\left(\kappa\sqrt{\cosh\left(zy_{\mathrm{D}}\right)}\right) \tag{5}$$

which is valid for a symmetric $z:z$ electrolyte, with $y_{\mathrm{D}} = F\psi_{\mathrm{D}}/RT$ the dimensionless Donnan potential defined by $y_{\mathrm{D}} = z^{-1}\mathrm{asinh}\left(z\rho_0/\left(2IF\right)\right)$ reached in the bulk shell layer (**Figure 1**) and asinh corresponds to the inverse hyperbolic sine function. The length scale $1/\kappa_{\mathrm{m}}$ basically refers to the distance over which the potential (in absolute value) decreases from $\left|y_{\mathrm{D}}\right|$ to the potential value at the interface formed with the outer electrolyte solution (i.e. at $r = r_{\mathrm{p}}$), as schemed in **Figure 1**. Eq. (5) highlights that the electrostatic potential distribution at the shell and water sides of the shell/solution interface becomes asymmetric for sufficiently charged soft systems, as $1/\kappa_{\mathrm{m}}$ differs from $1/\kappa$ with increasing the magnitude of the Donnan potential, and a similar conclusion holds with increasing electrolyte valence z. In turn, a Donnan phase is actually effective within the particle shell provided that the shell thickness δ is significantly larger than the intraparticulate screening distance, i.e. $\kappa_{\mathrm{m}}\delta \gg 1$. As the inequality $\kappa_{\mathrm{m}} \geq \kappa$ (cf. Eq. (5)) is always verified, the true condition $\kappa_{\mathrm{m}}\delta \gg 1$ underlying the applicability of a Donnan potential in the particle shell is commonly replaced by $\kappa\delta \gg 1$, which has the merit to be independent of y_{D}.

2.3. Conditional existence of a Donnan potential with account of steric effects.

Following Lesniewska et al. [60], the steric effects governed by the excluded volumes of ions and shell charges may significantly modulate the electrostatic potential distribution at soft interfaces, as compared to predictions from classical mean-field PB equation where ions and shell charges are assumed to be point-like. In addition, the screening of the shell charges by electrolyte ions can be either stronger or weaker than that expected from standard point-like electrostatic theory, depending on the respective magnitudes of the steric descriptors of the counterions, coions, and shell charges [60]. Accordingly, we

address below how these molecular properties of the electrolyte and shell component of the particle affect the establishment of a Donnan potential. For that purpose, we develop hereafter the expression of the electric double layer thickness that is operative within the shell (§2.3.2) so as to derive the condition that guarantees the existence of a Donnan phase within the soft layer with account of molecular steric effects. Prior to this, we formulate the additional condition required for y_{D} to be defined in a region where the electrostatic field is zero (§2.3.1).

2.3.1. Impact of steric effects on the neutralization of shell charges by electrolyte counterions in a Donnan phase.

Several reports on the electrostatics of soft interfaces provided expressions for the Donnan potential with account of steric effects mediated by electrolyte ions [58-60]. To the best of our knowledge, they are however valid only for symmetrical electrolytes and point-like structural charges. Despite of their limited applicability in e.g. complex biological media, these formulations of y_{D} evidence that the finite size of the ions can, in some cases, prevent the development of a Donnan potential within a given charged soft material as a result of constrained accumulation of the counterions therein, even for situations where $\kappa\delta \gg 1$. Notably, in our previous report [60] we demonstrated that the existence of a Donnan potential is tied to the verification of the inequality $1-\nu\left|n_0\right| z>0$ that involves the (dimensionless) density of structural charges in the shell, defined by $n_0=\rho_0/\left(2IF\right)$, and the bulk volume fraction of electrolyte ions, ν. In order to extend this result to more realistic cases where finite size of the shell charges may, in addition to ion steric effects, contribute to limit the accumulation of counterions in the shell, we start from the transcendental equation that governs the magnitude of the Donnan potential

$$n_0=\frac{n_{-}\left(y_{\mathrm{D}}\right)-n_{+}\left(y_{\mathrm{D}}\right)}{\left(z_{-}+z_{+}\right)} \tag{6}$$

which derives from the modified soft Poisson-Boltzmann equation (**SMFPB** Eq. (2)) taken in the limit of zero-electrostatic field in the shell. The spatial condition required for such an intra-shell zero-field condition to be achieved will be specifically elaborated in §2.3.2. Then, combining Eq. (6) with Eqs. (3) and (4), it is shown after some algebra that y_{D} is governed by the following expression valid for symmetrical electrolytes ($a_{+,-}=a$, $z_{+,-}=z$)

212 $$y_{\mathrm{D}} = z^{-1}\left[\operatorname{asinh}\left(\frac{\frac{\nu n_0 z}{1-a_{\mathrm{fix}}^3 c_{\mathrm{fix},0}}}{\sqrt{1-\left(\frac{\nu n_0 z}{1-a_{\mathrm{fix}}^3 c_{\mathrm{fix},0}}\right)^2}}\right)+\operatorname{asinh}\left(\frac{\frac{(1-\nu) n_0 z}{1-a_{\mathrm{fix}}^3 c_{\mathrm{fix},0}}}{\sqrt{1-\left(\frac{\nu n_0 z}{1-a_{\mathrm{fix}}^3 c_{\mathrm{fix},0}}\right)^2}}\right)\right] \quad (7)$$

213 where the nondiluteness parameter $\nu = \sum_{\text{ion } i} a_i^3 c_i^{\infty}$ reduces to $\nu = 2a^3 z c_0$. It is verified that Eq. (7)
214 simplifies into $y_{\mathrm{D}}\big|_{\nu=0} = z^{-1}\operatorname{asinh}(n_0 z)$ for $\nu = 0$, which correctly corresponds to the classical expression of
215 the Donnan potential recalled in §2 for symmetrical electrolytes with assimilating charges to immaterial
216 points in both electrolyte and shell layer ($a_{+,-} \to 0$ or, equivalently, $\nu = 0$, and $a_{\mathrm{fix}} \to 0$, respectively)
217 [45,62]. Eq. (7) makes it transparent that y_{D} is properly defined provided that $1 - \nu|n_0|z / \left(1 - a_{\mathrm{fix}}^3 c_{\mathrm{fix},0}\right)$ is
218 strictly positive, which corresponds to the generalization of our previous result $1 - \nu|n_0|z > 0$ [60] to
219 situations where the excluded volume of the structural shell charges is accounted on top of that of the
220 electrolyte ions. Adopting the 3D representation ($n_0 z$; $a_{\mathrm{fix}}^3 c_{\mathrm{fix},0}$; ν) to identify the existence domain of the
221 Donnan potential, **Figure 2** displays the envelop of equation $1 - \nu|n_0|z / \left(1 - a_{\mathrm{fix}}^3 c_{\mathrm{fix},0}\right) = 0$ which defines a
222 vertical asymptote for the behaviour of y_{D} versus $n_0 z$ at given $a_{\mathrm{fix}}^3 c_{\mathrm{fix},0}$ and ν (cf. Eq. (7)) : this existence
223 domain of y_{D} then simply corresponds to the points of coordinates ($n_0 z$; $a_{\mathrm{fix}}^3 c_{\mathrm{fix},0}$; ν) located below the
224 represented 2D envelop. As a brief recall of previous findings valid for $a_{\mathrm{fix}} = 0$ [60], **Figure 2** shows that
225 with increasing $|n_0|z$, y_{D} is defined for decreasing values of ν. Stated differently, the larger is the amount
226 of structural charges in the shell, the larger is the amount of counterions required to neutralize these
227 charges and, for that very neutralization purpose, the smaller the size of the counterions must be to fit in
228 the overall volume of the shell. With the additional account of the finite size $a_{\mathrm{fix}} > 0$ of the shell charges,
229 **Figure 2** evidences that an increase in a_{fix} lowers the maximum value of $|n_0|z$ for which y_{D} can be
230 achieved. In line with expectation, this constrain is most pronounced at large $|n_0|z$, i.e. for cases where
231 steric effects mediated both by electrolyte ions and shell charges most severely limit the development of
232 a Donnan potential in the shell particle component.

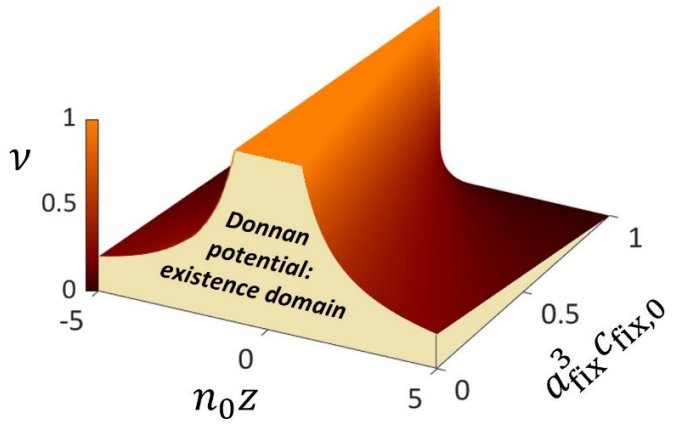

Figure 2. Existence domain of a Donnan potential for a symmetrical electrolyte containing cations and anions of similar size and valence, a and z, respectively, within the 3D representation $(n_0 z\,; a_{\text{fix}}^3 c_{\text{fix},0}\,; \nu)$. This existence domain (specified in the figure) is materialized by the yellow volume located under the represented envelope defined by the equation $1-\nu|n_0|z/\left(1-a_{\text{fix}}^3 c_{\text{fix},0}\right)=0$, with $n_0=\rho_0/(2IF)$ the dimensionless charge density in the shell, $\nu=2a^3 z c_0$ the parameter reflecting the nondiluteness of the electrolyte, and $c_{\text{fix},0}=|\rho_0|/Ze$ the number density of shell charges with effective volume a_{fix}^3 and valence Z.

233

234 For asymmetric electrolytes containing cations and anions of different valence and size, the derivation
235 of a closed form expression for y_{D} is not possible and numerical solving of Eq. (3), (4) and (6) along the
236 lines set forth in [60] is required to evaluate y_{D} and, therewith, identify the ranges of ion sizes and
237 valences, and values of density and size of shell charges where y_{D} is defined. For such electrolytes,
238 Lesniewska et al. [60] evidenced a similar limitation in the accumulation of ions due to steric effects (cf.
239 **Figure 2**) with a dominant role played by the excluded volumes of the counterions. The Donnan potential
240 will be thus evaluated in §3 as a function of n_0, $a_{+,-}$, $z_{+,-}$ and a_{fix} using a PTC Mathcad Prime 8.0
241 algorithm based on Levenberg-Marquardt method to solve y_{D} from Eqs. (3), (4) and (6). The domain of
242 existence of y_{D}, as constrained by the capability of the counterions to neutralize shell charges due to
243 their excluding volumes and that of the shell charges, will then be specified from location of the vertical
244 asymptotes of the simulated y_{D} values plotted versus n_0 for prescribed values of the nondiluteness
245 parameter, the density and size of shell structural charges. As argued for symmetrical electrolytes, this
246 asymptote corresponds to the critical physical situation where the volume of the shell is about to be
247 insufficient for hosting enough counterions to properly neutralize the structural charges distributed
248 therein and, thereby, cancel the electrostatic field.

249

2.3.2. Condition for the establishment of a zero-electrostatic field region within the shell layer.

The condition for the existence of y_D as invoked in the preceding section §2.3.1 is derived with – as a starting point – the SMFPB equation modified for steric effects and taken in the limit of zero-electrostatic field in the shell material. As discussed in §2.2, this latter limit is tied to the verification of the (additional) condition that the shell layer thickness must exceed the screening Debye layer $1/\kappa_m$ that is operative in the shell material [62,63]. The expression of $1/\kappa_m$ is elaborated here for an uncharged particle core surface, i.e. $\mathrm{d}y(r)/\mathrm{d}r\big|_{r=r_c} = 0$, because there is no electrostatic contribution from the core surface to the overall potential drop at the very shell/solution interface for the Donnan situations of interest. Then, considering that the potential 'deep' inside the shell reaches Donnan potential value, i.e. $y\left(r \to r_c^+\right) \approx y_D$, we search for the spatial dependence of the potential distribution $\Delta y(r) = y(r) - y_D$ for positions ranging from r_c up to the outer layer surface ($r \to r_p^-$). In turn, adopting an approach similar to that used by Ohshima [62], we seek to characterise at which distance from the surface layer the potential deviates from y_D (**Figure 1**). Substituting $y(r) = \Delta y(r) + y_D$ in the modified SMFPB Eqs. (2)-(4) that define the potential and ion densities distributions, it is shown that the dependence of $\Delta y(X)$ on position for the most generic case of asymmetrical electrolytes ($a_{+,-}$, $z_{+,-}$) is governed – up to second order term in Δy – by the following second order differential equation

$$\mathrm{d}^2\Delta y(X)/\mathrm{d}X^2 = \left(\kappa_m/\kappa\right)^2 \Delta y(X) \tag{8}$$

where κ_m is defined by

$$\kappa_m = \kappa\sqrt{\frac{\left(1-a_{fix}^3 c_{fix,0}\right) f_{cc}\left(y_D\right)\left[z_+ \mathrm{e}^{-z_+ y_D}\left(\nu \mathrm{e}^{z_- y_D} + 1 - \nu\right)^2 + z_-\left(1-\nu\right) g_{cc}\left(y_D\right)\mathrm{e}^{z_- y_D}\right]}{\left(z_+ + z_-\right)\left(g_{cc}\left(y_D\right)\right)^2\left(a_-^3 c_-^\infty \mathrm{e}^{z_- y_D} + 1 - \nu\right)}} \tag{9}$$

which is valid for $a_+ \geq a_-$. The defining expression of κ_m for cases where $a_+ \leq a_-$ is obtained by interchanging $\mathrm{e}^{z_- y}$ and $\mathrm{e}^{-z_+ y}$ and the subscripts '+' and '-' in Eq. (9). It is recalled that y_D in Eq. (9) is given by the numerical solution of Eqs. (3), (4) and (6) (cf. §2.3.1). We further verify that Eq. (9) correctly reduces to Eq. (5) applicable to point-like ions and shell charges, i.e. $a_{+,-} \to 0$, $a_{fix} \to 0$, and symmetrical electrolytes ($z_{+,-} = z$). For the sake of further comparison between situations where steric effects are and are not accounted for (cf. §3), we denote hereafter as $\kappa_{m,ref} = \kappa\sqrt{\cosh\left(zy_D\right)}$ (Eq. (5)) the reciprocal of the

intra-shell Debye length originally formulated by Ohshima [62] for symmetrical electrolytes and point-like charges.

For symmetrical electrolytes defined by $z_{+,-}=z$ and $a_{+,-}=a$, Eq. (9) simplifies into

$$\kappa_{\mathrm{m}}=\kappa\sqrt{\frac{\left(1-a_{\mathrm{fix}}^{3}c_{\mathrm{fix},0}\right)\left[\left(1-\nu\right)\cosh\left(zy_{\mathrm{D}}\right)+\nu\right]}{\left[\nu\cosh\left(zy_{\mathrm{D}}\right)+\left(1-\nu\right)\right]^{2}}} \tag{10}$$

where y_{D} is given by Eq. (7). While Eq. (7) involves the joint contributions of the nondiluteness of the electrolyte and of the excluded volume of the shell charges on y_{D}, Eq. (10) highlights that the Debye layer thickness within the shell, and therewith the electrotactic field at the very shell/solution, is also impacted by steric effects. For immaterial ions ($a_{+,-}\to 0$), both Eqs. (9) and (10) reduce to $\kappa_{\mathrm{m}}=\kappa\sqrt{\left(1-a_{\mathrm{fix}}^{3}c_{\mathrm{fix},0}\right)\cosh\left(zy_{\mathrm{D}}\right)}$, which pinpoints clearly that the finite excluded volume $a_{\mathrm{fix}}^{3}c_{\mathrm{fix},0}$ of the shell charges is able to generate some asymmetry between the potential distributions at the shell and solution sides of the shell/solution interface. In addition, the presence of the term $f_{\mathrm{cc}}\left(y_{\mathrm{D}}\right)$ in Eq. (9) reveals that differentiated sizes of the counterions and coions can also contribute to the asymmetry in the potential distribution at the shell/solution interface. In the limit of highly diluted shell component ($c_{\mathrm{fix},0}\to 0$, implying $y_{\mathrm{D}}\to 0$), Eq. (9) reduces (for $a_{+}\geq a_{-}$) to

$$\kappa_{\mathrm{m}}^{-1}\underset{c_{\mathrm{fix},0}\to 0}{\sim}\kappa^{-1}/\sqrt{\frac{z_{+}+\left(1-\nu\right)z_{-}}{\left(z_{+}+z_{-}\right)\left(1-a_{+}^{3}c_{+}^{\infty}\right)}}\equiv\kappa_{\mathrm{mod}}^{-1} \tag{11}$$

which is nothing else than the effective Debye layer thickness operative at the electrolyte side of particle/electrolyte interface and corrected here for ions-mediated steric effects. To avoid confusion, we denote as $\kappa_{\mathrm{mod}}^{-1}$ this modified Debye length pertaining to the solution side of the particle/solution interface. Eq. (11) correctly identifies with the expression given in [60] (Eq. (13) therein). In line with expectation, we have $\kappa_{\mathrm{mod}}^{-1}\to\kappa^{-1}$ for $\nu\to 0$ and, remarkably, this limit $\kappa_{\mathrm{mod}}^{-1}\to\kappa^{-1}$ also applies to the situation $a_{+}=a_{-}$. For cases where $a_{+}\neq a_{-}$, Eq. (11) implies the inequality $\kappa_{\mathrm{mod}}^{-1}\leq\kappa^{-1}$ (a typo mistake in [60] incorrectly indicates the reverse inequality), i.e. the screening Debye length is systematically overestimated if using the expression of κ^{-1} for situations where ion size ratio differs from unity.

For sake of completeness, from Eq. (8), it is straightforward to verify that the potential inside the polyelectrolyte shell can be approximated by $y\left(r\right)=y_{\mathrm{D}}+\left(y_{\mathrm{o}}-y_{\mathrm{D}}\right)\sinh\left(\kappa_{\mathrm{m}}\left(r-r_{c}\right)\right)/\sinh\left(\kappa_{\mathrm{m}}\delta\right)$, where $y_{\mathrm{o}}=y\left(r=r_{\mathrm{p}}\right)$ is the potential reached at the outer layer surface. Starting from Eqs. (1)-(4) linearized for

low potentials $y(r)(\ll 1)$, performing a first integration of the corresponding form of Eq. (2) to evaluate the electric field at both sides of the shell/solution interface ($r = r_p^-$ and $r = r_p^+$), and finally applying the continuity condition for the potential and field at $r = r_p$, we obtain, for $a_+ \geq a_-$,

$$y_o = y_D - \frac{y_D^2\left(1 - a_{fix}^3 c_{fix,0}\right)}{2n_0}\left[\frac{z_+ + (1-\nu)z_-}{(z_+ + z_-)\left(1 - a_+^3 c_+^\infty\right)}\right] \equiv y_D - \frac{y_D^2\left(1 - a_{fix}^3 c_{fix,0}\right)}{2n_0}\left(\frac{\kappa_{mod}}{\kappa}\right)^2 \quad (12)$$

where κ_{mod}^{-1} is defined by Eq. (11). Eq. (12) reduces to $y_o = y_D/2 = n_0/2$ for $z_+ = z_-$, $a_{+,-} \to 0$ and $a_{fix} \to 0$, in agreement with point-like results by Ohshima applicable to *z*:*z* electrolytes [62]. Remarkably, using the relationship $y_D = n_0\left(\kappa/\kappa_{mod}\right)^2 / \left(1 - a_{fix}^3 c_{fix,0}\right)$ between y_D and n_0, which is derived from Eq. (6) linearized up to first order term in y_D, Eq. (12) simplifies into $y_o = y_D/2$ for any $a_{+,-}$, $z_{+,-}$ and a_{fix}.

As an intermediate conclusion, the results provided in §2.3 define the conditional existence of a Donnan potential, which is tied to the verification of two criteria: one of these criteria ensures that the required neutralization of the shell charges by counterions, necessary to achieve the Donnan potential value y_D, is not limited by the excluded volumes of the ions and shell charges (cf. §2.3.1 and **Figure 2** that illustrates the case of symmetrical electrolytes), and the other criterion $\kappa_m \delta \gg 1$, with κ_m defined by Eq. (9), relates to the needed condition for the establishment of a zero-electrostatic field region within the shell layer. In the following section, computational examples are reported for a comprehensive evaluation of both the magnitude and domain of existence of Donnan potential in the shell, depending on the valence and size of the electrolyte counterions and coions, and on the excluded volume of the structural shell charges.

3. Results and discussion.

In this section, we address the existence domain of a Donnan phase within soft surface layers for a comprehensive set of electrolyte and soft layer electrostatic settings, which includes cases of similar or differentiated cation/anion valences and sizes. For that purpose, the evolution of y_D is computed for increasing values of the structural charge density n_0 of the shell, which in turn allows the specification of the critical values of n_0 for which the congestion of ions within the shell reaches a limit due to their incompressible volumes. Given the definition $n_0 = \rho_0/(2IF)$, we emphasize that increasing values of $|n_0|$ refer to an increase in the shell charge density (in absolute value) and/or a decrease in the solution ionic strength I, while all remaining parameters ($a_{+,-}^3 c_0$, $z_{+,-}$, and $a_{fix}^3 c_{fix,0}$) are kept constant. In addition, y_D

is systematically compared to $y_D|_{\nu=0}$ that refers to the standard point-like situation where $a_{+,-,fix} \to 0$. As argued in §2, a complete assessment of the existence domain of y_D further calls for the comparison of the spatial scale $1/\kappa_m$ with the shell layer thickness δ. Accordingly, for each analysed combination of ions and shell descriptors, we hereafter report the dimensionless ratio $\kappa_m^{-1}/\kappa^{-1}$ in the n_0-interval where y_D is properly defined, the ratio $\kappa_m^{-1}/\kappa^{-1}$ offering the advantage to assess the difference between screening distance inside and outside the shell (and therewith the asymmetry of the potential distribution at the shell/solution interface). To help physical interpretation of simulations, this ratio is further compared to the ratio $\kappa_{m,ref}^{-1}/\kappa^{-1}$ (Eq. (5)) formulated by Ohshima for symmetrical electrolytes and point-like ions and shell charges.

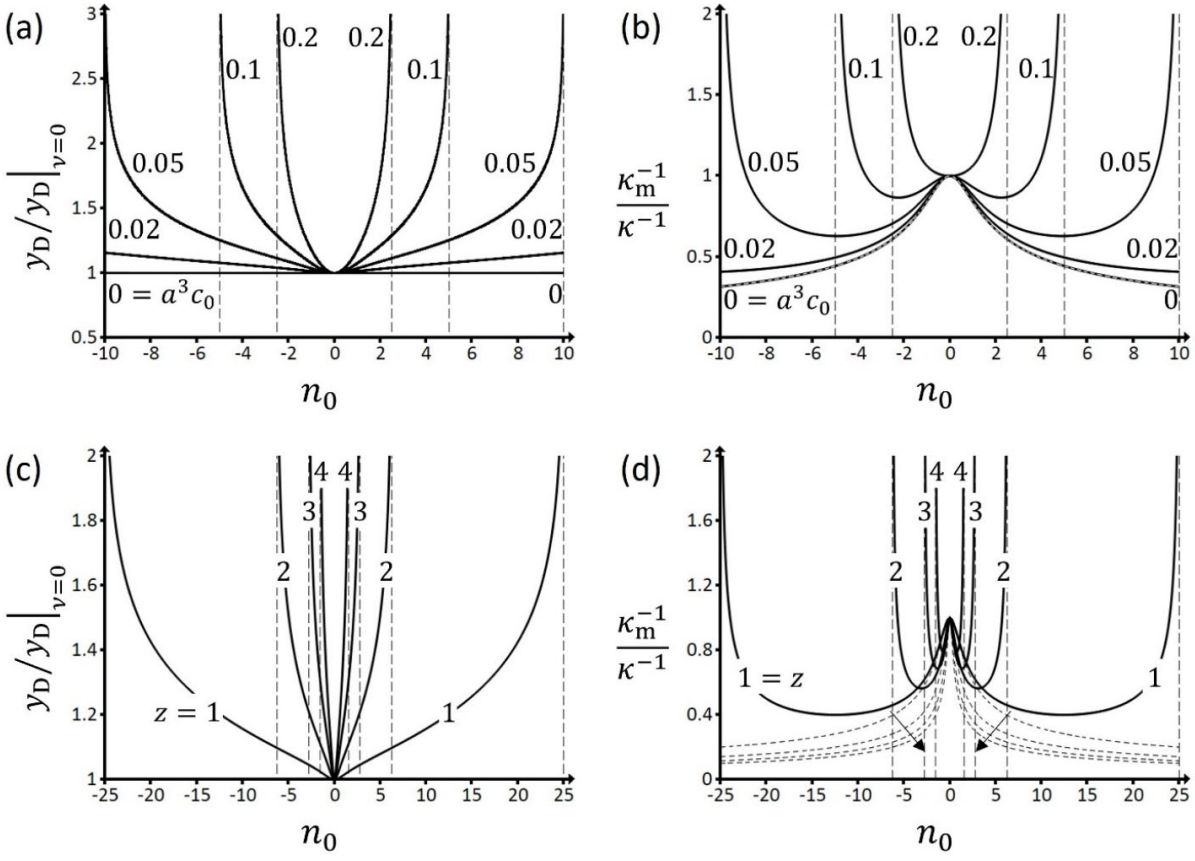

Figure 3. Donnan potential and Debye screening lengths ratios, $y_D/y_D|_{\nu=0}$ **(a,c)** and $\kappa_m^{-1}/\kappa^{-1}$ **(b,d)**, respectively, as a function of the dimensionless shell charge density n_0 for soft surface layers in contact with a symmetrical aqueous electrolyte defined by **(a,b)** $z_{+,-} = z = 1$ and different ion volumes a^3c_0 (indicated) with $a = a_{+,-}$, and **(c,d)** $a^3c_0 = 0.02$ and different ion valences z (indicated). Results are here given with neglecting steric effects connected to the size of shell charges, i.e. $a_{fix}^3 c_{fix,0} \to 0$. The dashed

curves in **(b,d)** correspond to $\kappa_{\mathrm{m,ref}}^{-1}/\kappa^{-1}$ (Eq. (5)), and the arrows in **(d)** point to increasing values of z with z = 1, 2, 3 and 4. The vertical dashed lines in all panels indicate the position $n_0 = n_0^*$ of the vertical asymptotes for $y_{\mathrm{D}}/y_{\mathrm{D}}\big|_{\nu=0}$ **(a,c)** and $\kappa_{\mathrm{m}}^{-1}/\kappa^{-1}$ **(b,d)** . For a given set of conditions examined, these asymptotes mark the frontier n_0^* of the n_0-domain below which a Donnan potential is defined within the shell layer, with $\left|n_0^*\right| = 1/(\nu z)$.

338

339 **Figure 3** shows the variations of $y_{\mathrm{D}}/y_{\mathrm{D}}\big|_{\nu=0}$ and $\kappa_{\mathrm{m}}^{-1}/\kappa^{-1}$ as a function of n_0 for symmetrical
340 electrolytes ($z_{+,-} = z$ and $a_{+,-} = a$) and, for the sake of demonstration, the steric effects due to the finite
341 size of the shell charges are here discarded ($a_{\mathrm{fix}}^3 c_{\mathrm{fix},0} \to 0$). For this situation, the results corresponding to
342 negatively ($n_0 < 0$) and positively ($n_0 > 0$) charged layers are symmetrical with respect to the axis $n_0 = 0$
343 , in agreement with the parity of the functions $y_{\mathrm{D}}/y_{\mathrm{D}}\big|_{\nu=0}$ and $\kappa_{\mathrm{m}}^{-1}/\kappa^{-1}$ (Eqs. (7) and (10)). For given z
344 and a, **Figure 3a** evidences that $y_{\mathrm{D}}/y_{\mathrm{D}}\big|_{\nu=0}$ is larger than unity over the whole range of n_0, and the
345 deviation of this ratio from unity increases with increasing $|n_0|$. This is so because the excluded volume of
346 the ions impairs their required accumulation in the shell for the establishment of a Donnan potential,
347 which in turn decreases the screening of the particle shell charges by the ions and increases the magnitude
348 of $y_{\mathrm{D}}/y_{\mathrm{D}}\big|_{\nu=0}$ (**Figure 2**). Accordingly, this increase of $y_{\mathrm{D}}/y_{\mathrm{D}}\big|_{\nu=0}$ becomes more important for increasing
349 values of the excluded volume of the ions at fixed value of $|n_0|$ (**Figure 3a**). The vertical asymptotes
350 appearing in the $y_{\mathrm{D}}/y_{\mathrm{D}}\big|_{\nu=0}$ vs. n_0 plots in **Figure 3a** are defined by the equation $n_0 = n_0^*$, with n_0^* marking
351 the frontier between the n_0-domains where y_{D} is and is not defined, i.e. $|n_0| < |n_0^*|$ and $|n_0| > |n_0^*|$,
352 respectively. The value of n_0^* and, therewith, the extension of the n_0-existence domain of y_{D} depends on
353 the nondiluteness of the bulk electrolyte and ion valence according to $\left|n_0^*\right| = 1/(\nu z)$, in agreement with
354 predictions from Eq. (7) that applies to symmetrical electrolytes (cf. **Figure 2**).
355 For point-like ions (i.e. $a^3 c_0 = 0$ or, equivalently, $\nu = 0$), **Figure 3b** confirms that $\kappa_{\mathrm{m}}^{-1}/\kappa^{-1}$ reduces to
356 $\kappa_{\mathrm{m,ref}}^{-1}/\kappa^{-1}$ (Eq. (5)), which corresponds to the outcome of Ohshima's model [62]. In details, $\kappa_{\mathrm{m,ref}}^{-1}/\kappa^{-1}$
357 decreases with $|n_0|$, in agreement with Eq. (5) that involves the Donnan potential defined, for point-like
358 ions, by $y_{\mathrm{D}}\big|_{\nu=0} = z^{-1}\mathrm{asinh}(n_0 z)$. This decrease in $\kappa_{\mathrm{m,ref}}^{-1}/\kappa^{-1}$ simply features that the drop of the potential
359 from y_{D} to y_{o} (surface potential of the shell layer defined by Eq. (12)) within the shell spans over a
360 distance shorter than that over which the potential drops in solution from y_{o} to 0 (**Figure 1**). In turn, the

potential distribution at the shell/solution interface features a marked asymmetry as the shell gets increasingly charged or, equivalently, y_D gets higher (in absolute value). Hereafter, we denote as 'y_D-*effect*' this effect that underlies a pronounced asymmetry of the potential distribution at the shell/solution interface as the shell gets increasingly charged (and $|y_D|$ larger). Like $\kappa_{m,ref}^{-1}/\kappa^{-1}$, the ratio $\kappa_m^{-1}/\kappa^{-1}$ decreases with $|n_0|$ for $\nu \ll 1$ (i.e. low a^3c_0) and/or sufficiently low $|n_0|$ (**Figure 3b**), basically because these conditions refer to a modest accumulation of the electrolyte ions inside the shell, i.e. the contribution of the excluded volume effects on ion partitioning is not dominant. For moderate values of the excluded ion volume a^3c_0 (i.e. $a^3c_0 = 0.05$ in **Figure 3b**), the monotonous decrease of $\kappa_m^{-1}/\kappa^{-1}$ with $|n_0|$ as achieved at lower a^3c_0 is replaced by a non-monotonous dependence with the apparition of a minimum at sufficiently low $|n_0|$. This minimum is the signature of a significant contribution of the excluded volume of the ions as they become increasingly packed within the shell to neutralize the structural shell charges. It is even so that for extreme values of a^3c_0, the underlying increasing branch of $\kappa_m^{-1}/\kappa^{-1}$ with $|n_0|$ dominates the overall dependence of $\kappa_m^{-1}/\kappa^{-1}$ on $|n_0|$ with the ensuing disappearance of the minimum invoked previously (cf. case $a^3c_0 = 0.2$ in **Figure 3b**). In other words, the larger is a^3c_0 (or ν) and/or $|n_0|$, the more the steric effects mediated by ions size dominate the impacts of the aforementioned 'y_D-effect' on $\kappa_m^{-1}/\kappa^{-1}$ which – if solely considered – would translate into a continuous decrease of $\kappa_m^{-1}/\kappa^{-1}$ with increasing $|n_0|$ or, equivalently, $|y_D|$. A noticeable consequence of such marked ions-related steric effects is that they may lead to a ratio $\kappa_m^{-1}/\kappa^{-1}$ which exceeds unity, a finding that cannot be predicted on the basis of point-like -based derivations [62] (Eq. (5)): steric effects then severely limit the screening power of the ions in moderate to highly charged shell layers as compared to that at the electrolyte side of the shell/solution interface. For extreme values of $|n_0|$, the resulting 'abrupt' increase in $\kappa_m^{-1}/\kappa^{-1}$ is materialized by a vertical asymptote $\kappa_m^{-1} \to \infty$, and this asymptote identifies with the $|n_0|$-boundary above which the Donnan potential y_D is no longer defined (cf. **Figure 3a**) due to severely constrained accumulation of ions within the shell. Last, for any fixed values of n_0, $\kappa_m^{-1}/\kappa^{-1}$ increases with the ion size a^3c_0, and it remains strictly superior to $\kappa_{m,ref}^{-1}/\kappa^{-1}$ (Eqs. (5) and (10)), as expected.

Figures 3c,d illustrate how the valence z of the counterions and coions of given volume fraction a^3c_0 affect the dependence of $y_D/y_D|_{\nu=0}$ (**Figure 3c**) and $\kappa_m^{-1}/\kappa^{-1}$ (**Figure 3d**) on $|n_0|$. In addition to the ion

size effect captured by **Figure 3a** and leading to increasing values of $y_D / y_D|_{\nu=0}$ with $|n_0|$, **Figure 3c** shows that $y_D / y_D|_{\nu=0}$ significantly increases with z at fixed $|n_0|$. In turn, the positioning of the vertical asymptotes $n_0 = n_0^*$ defining the existence domain of the Donnan potential (i.e. $|n_0| < |n_0^*|$), is shifted to lower values of n_0^* in agreement with $|n_0^*| = 1/(\nu z) = 1/(2a^3 c_0 z)$ applicable to symmetrical electrolytes. **Figure 3d** shows that at low $|n_0|$ and $\nu \ll 1$ ($a^3 c_0 = 0.02$ is adopted in **Figures 3c,d),** $\kappa_m^{-1} / \kappa^{-1}$ decreases with $|n_0|$ and correctly follows the predictions by Eq. (5) (cf. dashed curves in **Figure 3d)**, in line with the manifestation of the 'y_D-effect' defined from the discussion of **Figure 3b**. This decrease of $\kappa_m^{-1} / \kappa^{-1}$ gets stronger with increasing z as the asymmetry of the potential distribution at the shell/solution interface is more pronounced for multivalent electrolytes, a feature that also emerges from Eq. (5) (cf. the argument of the hyperbolic cosine function in Eq. (5)). For larger $|n_0|$, and similarly to **Figure 3b**, the excluded volume of the ions lead to a minimum in the curves $\kappa_m^{-1} / \kappa^{-1}$ versus n_0, and this minimum marks the onset of establishment of the vertical asymptote for $\kappa_m^{-1} / \kappa^{-1}$. In further agreement with **Figure 3c**, the threshold value $|n_0^*|$ defining this asymptote decreases significantly as ion valence gets higher: qualitatively, z acts on $y_D / y_D|_{\nu=0}$ and $\kappa_m^{-1} / \kappa^{-1}$ in a way comparable to that discussed for the ion volume $a^3 c_0$ in **Figures 3a,b**. In the scenario treated by **Figures 3c,d**, the increase of the individual charge carried by the ions thus drives a higher accumulation of the counterions in shells defined by low charge density $|n_0|$, which tends to increase the screening of the potential within the shell and to decrease $\kappa_m^{-1} / \kappa^{-1}$ ('y_D-effect'). At larger $|n_0|$, ion steric effects become important and ultimately generate the vertical asymptote $\kappa_m^{-1} \to \infty$, which reflects a significant decrease in the screening of the electrolyte ions in the shell. The valence z thus effectively increases the excluded volume of the ions which is given by $a^3 c_0 z$ [60]. In turn, steric exclusion of counterions from the shell is enhanced for multivalent electrolytes, which significantly lowers the corresponding $|n_0^*|$-boundary that defines the existence domain of y_D.

Overall, getting back to the condition $\kappa_m \delta \gg 1$ for establishment of a Donnan phase, an increase in size and/or valence of the ions of a given symmetrical electrolyte basically leads to an increase in the minimum layer thickness required for the potential distribution to reach a Donnan plateau value y_D (when defined) in comparison to classical point-like predictions (result valid for significantly charged

414 particle shell). This condition adds to the fulfilment of the criterion $|n_0| < 1/(\nu z)$ defining the existence

415 domain of y_D (**Figure 2)**.

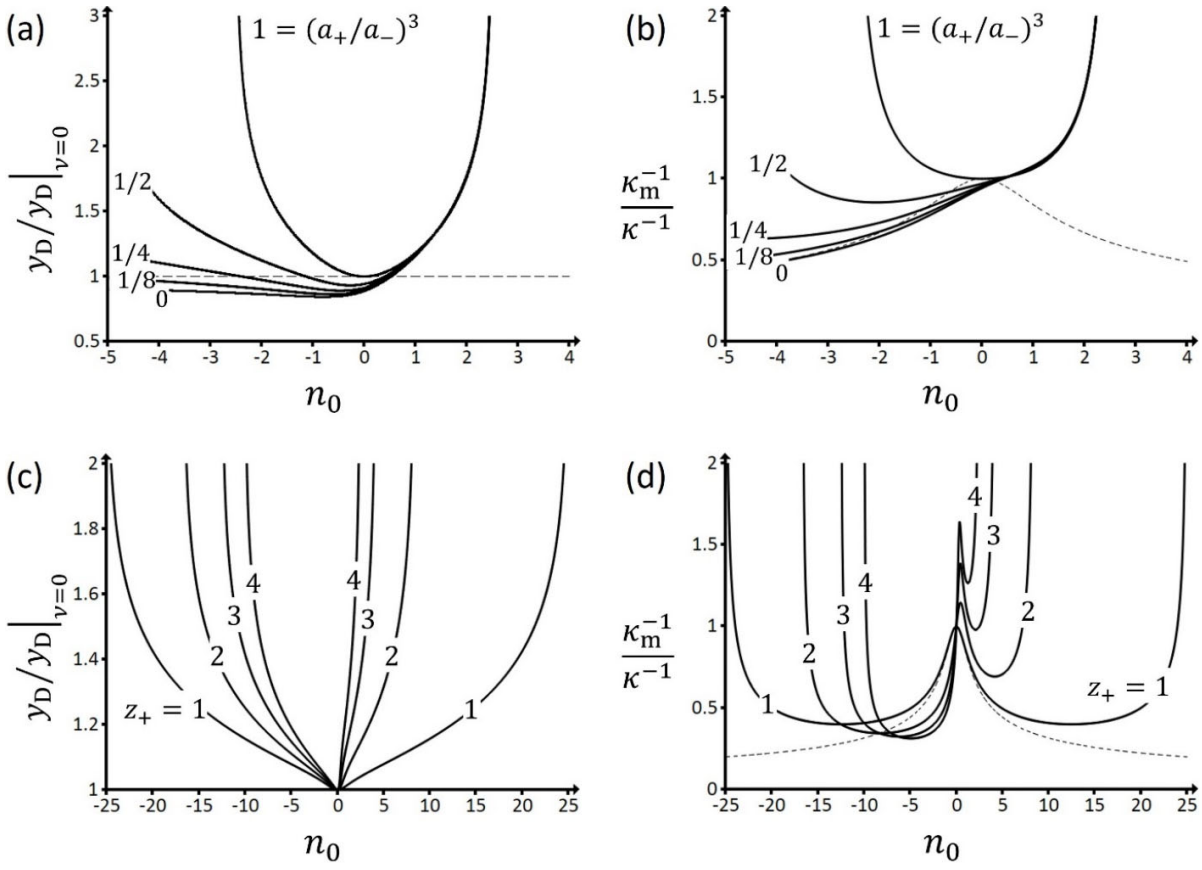

Figure 4. Donnan potential and Debye screening lengths ratios, $y_D / y_D|_{\nu=0}$ **(a,c)** and $\kappa_m^{-1} / \kappa^{-1}$ **(b,d)**, respectively, as a function of the dimensionless structural charge density n_0 for soft surface layers in contact with asymmetrical electrolytes defined by : **(a,b)** $z_{+,-} = 1$ and different cation/anion volume ratios $(a_+ / a_-)^3$ (indicated) at fixed anion size $a_-^3 c_0 = 0.2$, and **(c,d)** $a_{+,-}^3 c_0 = 0.02$ and different cation valences z_+ (indicated) at fixed anion valence $z_- = 1$. Results are here given with neglecting the steric effects connected to the size of the shell charges, i.e. $a_{fix}^3 c_{fix,0} \to 0$. Dashed curves in **(b,d)** refer to the ratio $\kappa_{m,ref}^{-1} / \kappa^{-1}$ (Eq. (5)) for $z_{+,-} = 1$. The horizontal dashed line in **(a)** helps the reader identifying the interval of n_0 values for which $y_D < y_D|_{\nu=0}$, depending on the ion size ratio a_+ / a_-.

416

417 For electrolytes where the cation/anion size ratio a_+ / a_- differs from unity, and further considering

418 $z_{+,-} = 1$ and $a_-^3 c_0 = 0.2$ (the latter condition marks a significant contribution of ions excluded volume, cf.

419 **Figures 3a,b**), **Figures 4a,b** evidence that the dependences of $y_D / y_D|_{\nu=0}$ and $\kappa_m^{-1} / \kappa^{-1}$ on n_0 become

strongly asymmetric, and the minimum reached by $y_D / y_D|_{\nu=0}$ (**Figure 4a**) is now shifted to higher $|n_0|$ with decreasing a_+ / a_-. Starting with the case $a_+ / a_- = 1$, a decrease in the size of the cations a_+ at fixed anion size a_- generates insignificant changes in $y_D / y_D|_{\nu=0}$ and $\kappa_m^{-1} / \kappa^{-1}$ for $n_0 > 0$ simply because the cations then act as coions and are thus the minor ionic species within the charged shell, and even more so as n_0 gets more positive. In contrast, a decrease of a_+ / a_- at fixed a_- leads to a decrease of the excluded volume effects pertaining to the counterions for negatively charged shell layers of given n_0 (and a companion increase of their screening of the shell charge), thereby lowering both $y_D / y_D|_{\nu=0}$ (**Figure 4a**) and $\kappa_m^{-1} / \kappa^{-1}$ (**Figure 4b)**. Remarkably, as long as $a_+ / a_- < 1$, the quantity $y_D / y_D|_{\nu=0}$ becomes lower than unity at sufficiently low $|n_0|$ and, within this range of $|n_0|$ values, $y_D / y_D|_{\nu=0}$ reaches a minimum for the reasons already invoked in **Figure 3a**. For $a_+ / a_- \to 0$ and very large $|n_0|$ in line with a complete exclusion of the coions (anions) from the negatively charged shell, the limit $y_D / y_D|_{\nu=0} \to 1$ is properly retrieved (not shown). As far as the ratio $\kappa_m^{-1} / \kappa^{-1}$ is concerned, it is lower than $\kappa_{m,ref}^{-1} / \kappa^{-1}$ (dashed curves in **Figure 4b**) over a range of $|n_0|$ values that expands upon lowering a_+ / a_-. In the limit $a_+ / a_- \to 0$, κ_m^{-1} correctly approaches the point-like limit $\kappa_{m,ref}^{-1}$ for $|n_0| \gg 1$ (with $n_0 < 0$) where coions are then entirely excluded from the shell layer. The above scenarios where $y_D / y_D|_{\nu=0} < 1$ and $\kappa_m^{-1} < \kappa_{m,ref}^{-1}$ (applicable for given ranges of $n_0 (< 0)$ and $a_+ / a_- < 1$ at fixed a_-) may appear counterintuitive as the point-like description of ions partitioning at the shell/solution interface should a priori refer to the situation where screening effects by the ions in the shell are most pronounced as their accumulation therein is not constrained by their size. However, the developments in §2.3.2 (Eq. (11)) evidenced that such screening effects are achieved not only for $a_{+,-} = 0$ but also for $a_+ = a_-$ at $|n_0| \ll 1$ recalling that the limit $\kappa_m^{-1} \to \kappa^{-1}$ is obtained under such conditions (**Figure 3b**). In turn, for ratios a_+ / a_- strictly lower than unity and at sufficiently low $|n_0|$, the screening power of the counterions in the shell is necessarily enhanced as compared to that expected on the basis of 'point-like' considerations, which leads to the aforementioned situations where $y_D / y_D|_{\nu=0} < 1$ and $\kappa_m^{-1} < \kappa_{m,ref}^{-1}$. The same argument explains the inequality $\kappa_{mod}^{-1} \le \kappa^{-1}$ given in §2.3.2.

In **Figures 4c,d**, we consider electrolytes where $a_+ = a_- (\neq 0)$ and we vary the value of $z_+ (\ge z_-)$ at fixed $z_- = 1$. While displaying – for a given z_+ – a dependence of $y_D / y_D|_{\nu=0}$ on $|n_0|$ that is qualitatively similar to that commented in **Figure 3c**, **Figure 4c** further shows that $y_D / y_D|_{\nu=0}$ increases with z_+ at fixed $|n_0|$.

For $n_0 < 0$ (range where cations are the counterions), the magnitude of this increase in $y_D / y_D|_{\nu=0}$ is significantly smaller than that observed for $n_0 > 0$, which generates a marked asymmetry of the plots $y_D / y_D|_{\nu=0}$ versus n_0 with respect to the line of equation $n_0 = 0$. This finding relates to the respective dependence of the excluded volumes of cations and anions defined by $a^3 c_+^\infty = a^3 c_0 z_-$ and $a^3 c_-^\infty = a^3 c_0 z_+$, respectively. In turn, increasing z_+ at fixed $a^3 c_0$ and fixed z_- will most significantly reduce the screening of the shell charge by electrolyte ions for $n_0 > 0$ where anions are the counterions. This is materialized by an increase of $y_D / y_D|_{\nu=0}$ with z_+ at given $|n_0|$ which is steeper for $n_0 > 0$ than it is for $n_0 < 0$, with a resulting reduction of the range of n_0 values where y_D is defined.

Figure 4d provides the ratio $\kappa_m^{-1} / \kappa^{-1}$ as a function of n_0 under the conditions examined in **Figure 4c**. For a negatively charged shell, starting from the reference situation $z_+ = z_- = 1$ already discussed in **Figure 3d**, the minimum reached by $\kappa_m^{-1} / \kappa^{-1}$ decreases here with increasing z_+ and is shifted to decreasing values of $|n_0|$. This change in the position of the minima with varying z_+ is consistent with the positioning of the vertical asymptotes defining the frontier of the n_0-domain where y_D exists in **Figure 4c**. The origin of the decrease of the minimum in $\kappa_m^{-1} / \kappa^{-1}$ with increasing z_+ is similar to that predicted by Eq. (5) for increasing values of the valence of symmetrical electrolytes. For $n_0 > 0$, the vertical asymptotes are again in agreement with the results provided in **Figure 4c,** and so is the positioning of the minima in $\kappa_m^{-1} / \kappa^{-1}$ with increasing z_+. The new feature is the increase of $\kappa_m^{-1} / \kappa^{-1}$ with increasing n_0 from 0 to $n_0 \sim 0.5$, and this increase is more important as z_+ gets higher. Then, similarly to the cases tackled in **Figure 3d**, $\kappa_m^{-1} / \kappa^{-1}$ decreases at larger n_0, and reaches a minimum that precedes the asymptotic behaviour at $n_0 = n_0^*$. The initial increase of $\kappa_m^{-1} / \kappa^{-1}$ at low (positive) n_0 stems from anions-excluded volume effects that are enhanced with increasing z_+ at fixed $a^3 c_0$ and z_-, as argued previously (cf. **Figure 4c**). For moderate values of n_0, the decrease in $\kappa_m^{-1} / \kappa^{-1}$ with n_0 (or y_D) is explained by a stronger asymmetry of the potential profiles at both sides of the shell/solution interface (the 'y_D-effect' captured by Eq. (5)). For extreme values of n_0, the steric limit of anions accumulation in the shell is approached, which gives rise to the increase of $\kappa_m^{-1} / \kappa^{-1}$ and to the associated apparition of the vertical asymptote.

As a last remark on **Figure 4** and following the discussion in §2.3.2 (cf. Eq. (11)), for electrolytes where cations and anions differ in size, κ_{mod}^{-1} may appear as a better descriptor (compared to κ^{-1}) of the electrical

double layer thickness operative at the electrolyte side of the shell/electrolyte interface. Therefore, we provide in **Figure S1** (**S**upplementary **M**aterial) the ratio $\kappa_{\mathrm{m}}^{-1}/\kappa_{\mathrm{mod}}^{-1}$ for some of the conditions examined in **Figures 4b,d**. Basically, there are no new features emerging from **Figure S1** while quantitative differences between data in **Figure S1** and **Figure 4b,d** are simply explained by the very dependence of $\kappa_{\mathrm{mod}}^{-1}$ on cations and anions sizes (cf. Eq. (11)). The reader is referred to **SM** for further details. For the sake of completeness, we mention that varying the size ratio $a_-/a_+\left(<1\right)$ at fixed a_+ for $z_->z_+$ and $z_+=1$ generate evolutions of $y_{\mathrm{D}}/y_{\mathrm{D}}\big|_{\nu=0}$ and $\kappa_{\mathrm{m}}^{-1}/\kappa^{-1}$ with n_0 that are the symmetric (with respect to the axis $n_0=0$) of those displayed in **Figure 4**, because roles of cations and anions are then interchanged.

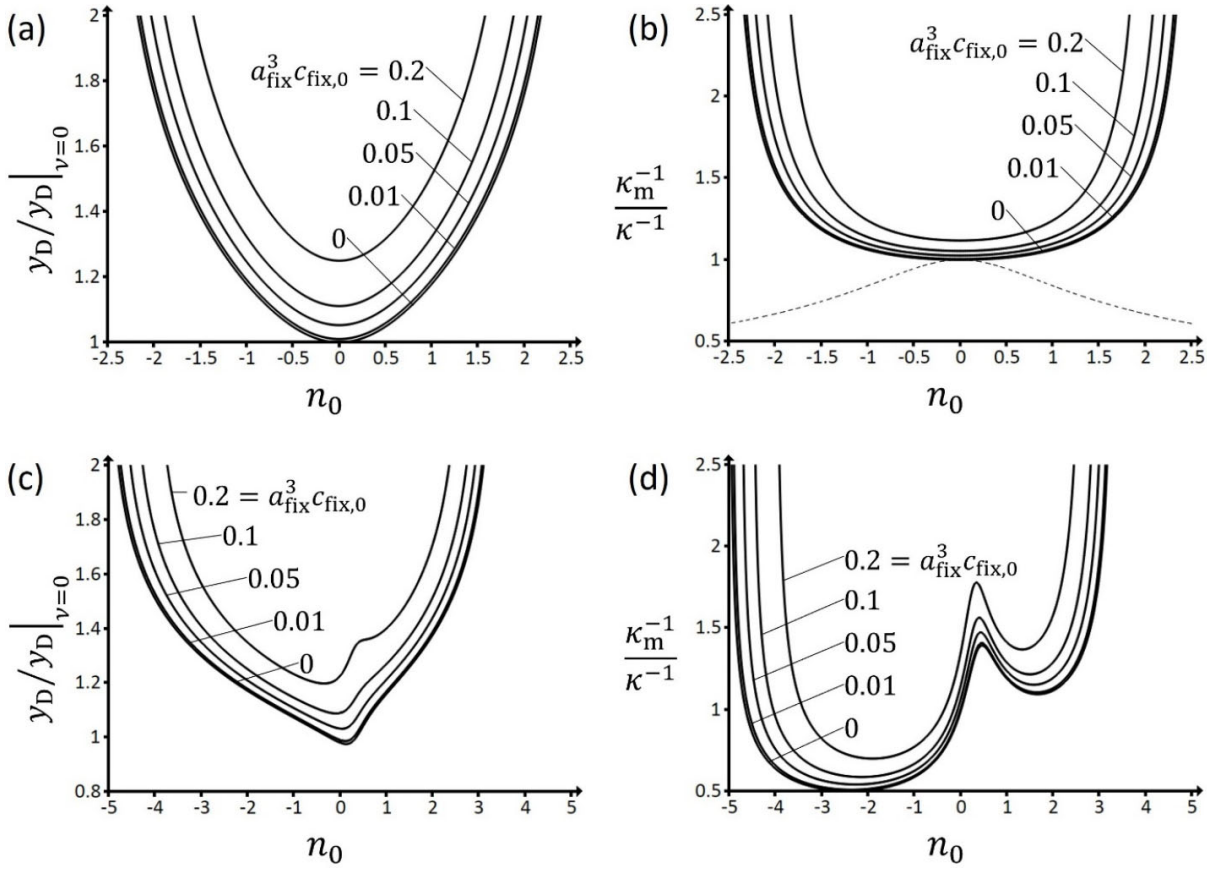

Figure 5. Donnan potential and Debye screening lengths ratios, $y_{\mathrm{D}}/y_{\mathrm{D}}\big|_{\nu=0}$ **(a,c)** and $\kappa_{\mathrm{m}}^{-1}/\kappa^{-1}$ **(b,d)**, respectively, as a function of the dimensionless structural charge density n_0 for soft surface layers whose charges are defined by a dimensionless excluded volume $a_{\mathrm{fix}}^3 c_{\mathrm{fix},0}$ (indicated), and which are in contact with: **(a,b)** a symmetrical electrolyte defined by $a^3 c_0 = 0.2$ and $z=1$, and **(c,d)** an asymmetrical

electrolyte defined by $z_- = 1$, $z_+ = 3$, $a_+^3 c_0 = 0.05$ and $a_-^3 c_0 = 0.025$. Dashed curve in **(b)** refers to the ratio $\kappa_{\mathrm{m,ref}}^{-1} / \kappa^{-1}$ (Eq. (5)) for $z_{+,-} = 1$.

Finally, **Figure 5** illustrates the impact of the excluded volume of the shell charges, $a_{\mathrm{fix}}^3 c_{\mathrm{fix},0}$, on $y_{\mathrm{D}} / y_{\mathrm{D}}\big|_{\nu=0}$ and $\kappa_{\mathrm{m}}^{-1} / \kappa^{-1}$ for both symmetrical (**Figures 5a,b**) and asymmetrical (**Figures 5c,d**) electrolytes in terms of cations/anions size and valence. For all treated cases, the shapes of the curves $y_{\mathrm{D}} / y_{\mathrm{D}}\big|_{\nu=0}$ and $\kappa_{\mathrm{m}}^{-1} / \kappa^{-1}$ versus n_0 conform to those discussed in **Figure 3** and **Figure 4** for $a_{\mathrm{fix}}^3 c_{\mathrm{fix},0} \to 0$ (symmetrical and unsymmetrical electrolyte conditions, respectively), and **Figure 5** shows that an increase in $a_{\mathrm{fix}}^3 c_{\mathrm{fix},0}$ leads to a shift of both $y_{\mathrm{D}} / y_{\mathrm{D}}\big|_{\nu=0}$ and $\kappa_{\mathrm{m}}^{-1} / \kappa^{-1}$ to larger values over the whole range of n_0 conditions. Indeed, larger volume fractions of structural charges in the shell necessarily imply lower densities of electrolyte ions therein (regardless of their valence and size), which reduces the screening of the shell charges by the ions accumulated therein. In turn, the account of a finite $a_{\mathrm{fix}}^3 c_{\mathrm{fix},0}$ systematically results in a narrower n_0-domain where a Donnan potential can be established in the shell, in agreement with e.g. the equation of the boundary $\left|n_0^*\right| = \left(1 - a_{\mathrm{fix}}^3 c_{\mathrm{fix},0}\right) / \left(\nu z\right)$ applicable to symmetrical electrolytes (cf. **Figure 2** and Eq. (7)).

4. Conclusions.

In this work, we discuss the conditional existence of a Donnan potential within a charged polyelectrolytic particle shell with explicit account of steric effects mediated by the size and valence of the electrolyte ions and the size of the structural charges carried by the shell. Based on recent corrections of mean-field Poisson-Boltzmann theory for steric effects [60], we develop a formalism that addresses both the existence and magnitude of the Donnan potential in the shell over a large spectrum of electrolyte conditions in terms of (a)symmetry of counterions/coions size and/or valence. The results evidence that a Donnan potential is achieved in a given shell layer pending the fulfilment of two criteria: (i) the accumulation of counterions in the shell leading to neutralization of the structural charges therein is not limited by steric effects, and (ii) the layer thickness is sufficient for the establishment of a zero-electric field region (the Donnan phase) in the particle shell. The first criterion (i) is defined from systematic evaluation of the dependence of the Donnan potential on a dimensionless shell charge density involving solution ionic strength, for various molecular properties of the electrolyte and shell layer. The method then identifies the conditions where shell charge neutralization is physically possible and those where it is not. The second criterion (ii) involves the characteristic screening Debye length operative in the shell

layer that we formulate explicitly as a function of the excluded volumes of the electrolyte ions and shell charges. In turn, a zero-electric field is reached in the shell provided that the shell thickness well exceeds this intra-shell screening Debye length. Additional comparison of criteria (i) and (ii) to outcomes where ions and shell charges are assimilated to immaterial points makes it further possible to identify and explain the situations where the Donnan potential and the magnitude of electrolyte screening is over- or under-estimated by classical mean field electrostatic theory for soft surfaces. To summarize, for symmetrical electrolytes (cations/anions featuring similar size *and* valence), the excluded volumes of the counterions in the shell lead to a decrease of screening of the shell charges, an increase in Donnan potential (in absolute value) and a reduction of the interval of shell density values for which a Donnan phase is established. These effects, depending on the magnitude of the Donnan potential and molecular descriptors of the electrolyte, may associate with a marked asymmetry of the potential distribution at the shell/solution interface. For asymmetrical electrolytes, the differentiated contributions of the excluded volumes pertaining to the counterions and coions may lead to situations where the shell charge screening exceeds the one predicted by point-like electrostatic theory.

Given the importance of Donnan theory for the electrostatics and electrokinetics of soft particles and soft macroscopic surfaces [62-64], the current work may be valuable to address the domain of validity of this theory, especially for biological particles under high salt concentration conditions where steric effects can be significant. In another context, binding of metal ions and protons to particulate organic matter is commonly evaluated by equilibrium Non-Ideal Competitive Adsorption (NICA)-Donnan model [65]. While the limits of that model have been identified and alternatives proposed [66,67], the results reported in this work allow a refined identification of the conditions underlying the applicability of the Donnan electrostatic framework depending on particle size and charge, solution ionic strength, size and valence of the background electrolyte ions. Future follow-up of this work includes the extension of the here-reported formalism to complex electrolyte mixtures – as required for the analysis of particle electrostatics in natural waters – so as to decipher the impacts of asymmetries in size and valence of the different types of involved coions and counterions on the overall ion-accumulation capacity of the particle soft component. Finally, it is believed that the formalism can offer a valuable mechanistic framework to analyse the partitioning of ions in hydrogels depending on outer electrolyte composition, which is required in e.g. polymer-based applications for the removal of contaminants in water and wastewater treatment [68].

CRediT authorship contribution statement.

Nicolas Lesniewska: Methodology, Software, Formal analysis, Validation, Investigation, Writing - original draft. **Audrey Beaussart**: Investigation, Writing - review & editing, Supervision. **Jérôme F.L. Duval**: Conceptualization, Methodology, Software, Formal analysis, Investigation, Writing - review & editing, Supervision.

Declaration of Competing Interest. The authors declare that they have no known competing financial interests or personal relationships that could have appeared to influence the work reported in this paper.

Supplementary material. Supplementary data to this article can be found online at https://doi.org/XXX.

552 **Glossary of symbols.**

553 **Latin symbols**

554 a_+, a_-, a_{fix} effective radii of cations, anions and shell charges (m), respectively

555 $c_+(r)$, $c_-(r)$ number densities of cations and anions (m^{-3}) at position r, respectively, with corresponding

556 bulk solution values defined by $c_+^{\infty} = c_0 z_-$ and $c_-^{\infty} = c_0 z_+$

557 $c_{\mathrm{fix}}(r)$ number density of shell charges at position r, defined by $c_{\mathrm{fix}}(r) = |\rho_{\mathrm{fix}}(r)| / (Ze)$

558 $c_{\mathrm{fix},0}$ defined by $c_{\mathrm{fix},0} = c_{\mathrm{fix}}(r = r_{\mathrm{c}})$

559 I solution ionic strength (mol m^{-3})

560 n_0 dimensionless density of structural charges in the shell

561 n_0^* frontier of the n_0-domain for which a Donnan potential is defined within a shell layer

562 $n_+(r)$, $n_-(r)$ dimensionless densities of cations and anions at position r, respectively

563 r radial coordinate (m)

564 r_{c} hard particle core radius (m)

565 r_{p} soft particle radius (m), with $r_{\mathrm{p}} = r_{\mathrm{c}} + \delta$

566 X dimensionless space variable defined by $X = \kappa(r - r_{\mathrm{c}})$

567 $y(r)$ dimensionless potential at position r

568 y_{D} dimensionless Donnan potential

569 y_{o} dimensionless potential at the position $r = r_{\mathrm{p}}$ (cf. Figure 1)

570 z_+, z_-, Z unsigned valences of cations, anions and shell charges respectively

571 **Greek symbols**

572 δ soft layer thickness (m)

573 ε_0 dielectric permittivity of vacuum (F m^{-1})

574 ε_{s} relative dielectric permittivity of the solvent (water)

575 $1/\kappa$ Debye length in solution, without account of steric effects (m)

576 $1/\kappa_{\mathrm{m}}$ Debye length operative in the shell region, with account of steric effects (m) (Eqs. (9)-(10))

577 $1/\kappa_{\mathrm{m,ref}}$ Debye length operative in the shell region, without account of steric effects (m) (Eq. (5))

578 $1/\kappa_{\mathrm{mod}}$ Debye length in solution corrected for ion steric effects (m) (Eq. (11))

579 ν measure of the nondiluteness of the electrolyte, $\nu = a_+^3 c_+^{\infty} + a_-^3 c_-^{\infty}$

580 ρ_0 density of structural charges homogeneously distributed within the shell (C m^{-3})

581 $\rho_{\text{fix}}(r)$ density of structural charges at position r (C m^{-3}), as defined by Eq. (1)

582 $\psi(r)$ electrostatic potential at position r (V)

583 **References.**

584 [1] J. Lyklema, Fundamentals of interface and colloid science. Volume IV: Particulate colloids, Chapter 3
585 Academic Press, London, 2005.
586 [2] C.Y. Son, Z.-G. Wang, Image-charge effects on ion adsorption near aqueous interfaces, Proc. Natl. Acad.
587 Sci. U.S.A 118 (2021) e2020615118.
588 [3] H. Ohshima, Theory of electrostatics and electrokinetics of soft particles, Sci. Technol. Adv. Mater.
589 (2009) 10, 063001.
590 [4] C.G. Lopez, T. Lohmeier, J.E. Wong, W. Richtering, Electrostatic expansion of polyelectrolyte microgels:
591 effect of solvent quality and added salt, J. Colloid Interface Sci. 558 (2020) 200-210.
592 [5] N. Tamura, S. Itoh, M. Nishimura, Existence of two types of electrostatic interaction in reactions
593 catalyzed by Ferredoxin-NADP oxidoreductase, Plant and Cell Physiology 25 (1984) 589-599.
594 [6] Y. Ma, K. Poole, J. Goyette, K. Gaus, Introducing membrane charge and membrane potential to T cell
595 signaling, Front. Immunol. 8 (2017) 1513.
596 [7] O. Alegun, A. Pandeya, J. Cui, I. Ojo, Y. Wei, Donnan potential across the outer membrane of Gram-
597 negative bacteria and its effect on the permeability of antibiotics, Antibiotics 10 (2021) 701.
598 [8] G. Laucirica, M.E. Toimil-Molares, C. Trautmann, W. Marmisollé, O. Azzaroni, Nanofluidic osmotic
599 power generators - advanced nanoporous membranes and nanochannels for blue energy harvesting.
600 Chem. Sci. 12 (2021) 12874-12910.
601 [9] P. Debye, H. Hückel, The theory of electrolytes. I. The lowering of the freezing point and related
602 occurrences, Physik. Z. 24 (1923) 185.
603 [10] A.R. Denton, Poisson-Boltzmann theory of charged colloids: limits of the cell model for salty
604 suspensions, J. Phys.: Condens. Matter 22 (2010) 364108.
605 [11] S. Levine, G.M. Bell, Theory of a modified Poisson-Boltzmann equation. I. the volume effect of
606 hydrated ions, J. Phys. Chem. 64 (1960) 1188-1195.
607 [12] C.W. Outhwaite, A modified Poisson–Boltzmann equation in electric double layer theory for a
608 primitive model electrolyte with size-asymmetric ions, J. Chem. Phys. 84 (1986) 3461.
609 [13] J.J. Lopez-Garcia, M.J. Aranda-Rascon, J. Horno, Electrical double layer around a spherical colloid
610 particle: The excluded volume effect, J. Colloid Interface Sci. 316 (2007) 196-201.
611 [14] A. Abrashkin, D. Andelman, H. Orland, Dipolar Poisson-Boltzmann equation: ions and dipoles close to
612 charge interfaces, Phys. Rev. lett. 99 (2007) 077801.
613 [15] P. Koehl, H. Orland, M. Delarue, Adapting Poisson-Boltzmann to the self-consistent mean field theory:
614 application to protein side-chain modelling, J. Chem. Phys. 135 (2011) 055104.
615 [16] D. Ben-Yaakov, D. Andelman, R. Podgornik, D. Harries, Ion-specific hydration effects: Extending the
616 Poisson-Boltzmann theory, Curr. Opin. Colloid Interface Sci. 16 (2011) 542-550.
617 [17] P.H.R. Alijo, F.W. Tavares, E.C. Biscaia Jr., Double layer interaction between charged parallel plates
618 using a modified Poisson-Boltzmann equation to include size effects and ion specificity, Colloids Surf. A
619 Physicochem. Eng. Asp. 412 (2012) 29-35.
620 [18] J.J. Lopez-García, J. Horno, C. Grosse, Influence of the finite size and effective permittivity of ions on
621 the equilibrium double layer around colloidal particles in aqueous electrolyte solution, J. Colloid Interface
622 Sci. 428 (2014) 308-315.
623 [19] Yu. A. Budkov, A.L. Kolesnikov, M.G. Kiselev, A modified Poisson-Boltzmann theory: effects of co-
624 solvent polarizability, EPL 111 (2015) 28002.

[20] R. M. Adar, T. Markovich, D. Andelman, Bjerrum pairs in ionic solutions: A Poisson-Boltzmann approach, J. Chem. Phys. 146 (2017) 194904.
[21] A. Gupta, H.A. Stone, Electrical double layers: effects of asymmetry in electrolyte valence on steric effects, dielectric decrement, and ion-ion correlations, Langmuir 34 (2018) 11971-11985.
[22] H. Sugioka, Expanded ion-conserving Poisson-Boltzmann theory at extremely-high voltages, Colloids Surf. A Physicochem. Eng. Asp. 630 (2021) 127667.
[23] J.-F. Dufrêche, V. Marry, O. Bernard, P. Turq, Models for electrokinetic phenomena in montmorillonite, Colloids Surf. A Physicochem. Eng. Asp. 195 (2001) 171-180.
[24] G. Le Breton, L. Joly, Molecular modeling of aqueous electrolytes at interfaces: Effects of long-range dispersion forces and of ionic charge rescaling, J. Chem. Phys. 152 (2020) 241102.
[25] X. Shen, I.C. Bourg, Molecular dynamics simulations of the colloidal interaction between smectite clay nanoparticles in liquid water, J. Colloid Interface Sci. 584 (2021) 610-621.
[26] H. Zhang, J. Zheng, C. Lin, S. Yuan, Molecular dynamics study on adsorption and desorption of lysozyme above polymer antifouling membranes, Colloids Surf. A Physicochem. Eng. Asp. 649 (2022) 129466.
[27] D.K. Deka, S. Pati, Electrocoalescence dynamics of two unequal-sized droplets, Colloids Surf. A Physicochem. Eng. Asp. 664 (2023) 131152.
[28] H.-Y. Zhang, R.J. Hill, Lipopolymer electrophoresis in supported bilayer membranes, Soft Matter, 6 (2010) 5625-5635.
[29] H. Ohshima, Electrophoresis of soft particles, Adv. Coll. Interface Sci. 62 (1995) 189-235.
[30] J.F.L. Duval, C. Werner, R. Zimmermann, Electrokinetics of soft polymeric interphases with layered distribution of anionic and cationic charges, Curr. Opin. Colloid Interface Sci. 24 (2016) 1-12.
[31] J.F.L. Duval, F. Gaboriaud, Progress in electrohydrodynamics of soft microbial particle interphases. Curr. Opin. Colloid Interface Sci. 15 (2010) 184-195.
[32] P.P. Gopmandal, J.F.L. Duval, Electrostatics and electrophoresis of engineered nanoparticles and particulate environmental contaminants: beyond zeta potential-based formulation, Curr. Opin. Colloid Interface Sci. 60 (2022) 101605.
[33] G. Bonacucina, M. Cespi, M. Misici-Falzi, G.F. Palmieri, Colloidal soft matter as drug delivery system, J. Pharm Sci. 98 (2009) 1-42.
[34] D. Jiang, X. Song, H. Zhang, M. Yuan, Removal of organic pollutants with polylactic acid-based nanofiber composites, Polymers 14 (2022) 4622.
[35] X. Xu, N. Bizmark, K.S.S. Christie, S.S. Datta, Z.J. Ren, R. D. Priestley, Thermoresponsive polymers for water treatment and collection, Macromolecules 55 (2022) 1894-1909.
[36] J. Bernal-Bayard, J. Thiebaud, M. Brossaud, A. Beaussart, C. Caillet, Y. Waldvogel, L. Travier, S. Létoffé, T. Fontaine, B. Rokbi, P. Talaga, C. Beloin, N. Mistretta, J.F.L. Duval, J.M. Ghigo, Bacterial capsular polysaccharides with antibiofilm activity share common biophysical and electrokinetic properties. Nat. comm. 14 (2023) 2553.
[37] R. Zimmermann, S.S. Dukhin, C. Werner, J.F.L. Duval, On the use of electrokinetics for unraveling charging and structure of soft planar polymer films. Curr. Opin. Colloid Interface Sci. 18 (2013) 83-92.
[38] J.F.L. Duval, D. Küttner, C. Werner, R. Zimmermann, Electrohydrodynamics of soft polyelectrolyte multilayers: point of zero-streaming current, Langmuir 27 (2011) 10739-10752.
[39] R.J. Hill, D.A. Saville, W.B. Russel, Electrophoresis of spherical polymer-coated colloidal particles, J. Colloid Interface Sci. 258 (2003) 56-74.
[40] J.J. Lopez-Garcia, C. Grosse, J.J. Horno, Numerical study of colloidal suspensions of soft spherical particles using the network method: 1. DC electrophoretic mobility, J. Colloid Interface Sci. 265 (2003) 327-340.

[41] J.F.L. Duval, J. Merlin, J., P.A.L. Narayana, Electrostatic interactions between diffuse soft multi-layered (bio)particles: beyond Debye-Hückel approximation and Deryagin formulation, Phys. Chem. Chem. Phys. 13 (2011) 1037-1053.
[42] H. Ohshima, Electrostatic interaction between soft particles, J. Colloid Interface Sci. 328 (2008) 3-9.
[43] H. Ohshima, Electrostatic interaction between two interpenetrating soft particles, Colloids Surf. A Physicochem. Eng. Asp. 460 (2014) 448-453.
[44] J.F.L. Duval, H. Ohshima, Electrophoresis of diffuse soft particles, Langmuir 22 (2006) 3533-3546.
[45] H. Ohshima, S. Ohki, Donnan potential and surface potential of a charged membrane, Biophys. J. 47 (1985) 673-678.
[46] A. Mauro, Space charge regions in fixed charge membranes and the associated property of capacitance, Biophys. J. 2 (1962) 179-198.
[47] J.F.L. Duval, H.P. van Leeuwen, Electrokinetics of diffuse soft interfaces. I. Limit of low Donnan potentials, Langmuir 20 (2004) 10324-10336.
[48] J.F.L. Duval, Electrokinetics of diffuse soft interfaces. II. Analysis based on the nonlinear Poisson-Boltzmann equation, Langmuir 21 (2005) 3247-3258.
[49] J.T. Davies, E.K. Rideal. 1961. Interfacial Phenomena. Academic Press, Inc., New York and London. 75-84.
[50] S. Ohki, Rectification by a double membrane, J. Phys. Soc. Jpn. 20 (1965) 1674-1685.
[51] P.A. Gokturk, R. Sujanani, J. Qian, Y. Wang, L.E. Katz, B.D. Freeman, E.J. Crumlin, The Donnan potential revealed, Nat. comm. 13 (2022) 5880.
[52] T.A. Davis, L.P. Yezek, J.P. Pinheiro, H.P. van Leeuwen, Measurement of Donnan potentials in gels by in situ microelectrode voltammetry, J. Electroanal. Chem. 584 (2005) 100-109.
[53] C. Pagnout, A. Razafitianamaharavo, B. Sohm, C. Caillet, A. Beaussart, E. Delatour, I. Bihannic, M. Offroy, M., J.F.L. Duval, Osmotic stress and vesiculation as key mechanisms controlling bacterial sensitivity and resistance to TiO2 nanoparticles, Commun. Biol. 4 (2021) 678.
[54] G. Goodwin, S. B. McMahon, The physiological function of different voltage-gated sodium channels in pain. Nat. Rev. Neurosci. 22 (2021) 263-274.
[55] I. Borukhov, D. Andelman, H. Orland, Steric effects in electrolytes: a modified Poisson-Boltzmann equation, Phys. Rev. Lett. 79 (1997) 435.
[56] A.G. Moreira, R.R. Netz, Strong coupling theory for counter-ion distributions, EPL 52 (2000) 705.
[57] T.-L. Horng, Review and modification of entropy modeling for steric effects in the Poisson-Boltzmann equation, Entropy 22 (2020) 632.
[58] S. Chanda, S. Das, Effect of finite ion sizes in an electrostatic potential distribution for a charged soft surface in contact with an electrolyte solution, Phys. Rev. E 89 (2014) 012307.
[59] P. Gopmandal, S. De, H. Ohshima, Impact of ion-steric and ion-partitioning effects on electrophoresis of soft particles, Phys. Rev. E 102 (2020) 032601.
[60] N. Lesniewska, A. Beaussart, J.F.L. Duval, Electrostatics of soft (bio)interfaces: corrections of mean-field Poisson-Boltzmann theory for ion size, dielectric decrement and ion-ion correlations, J. Colloid Interface Sci. 642 (2023) 154-158.
[61] M.S. Kilic, M.Z. Bazant, Steric effects in the dynamics of electrolytes at large applied voltages. I. Double-layer charging, Phys. Rev. 75 (2007) 021502.
[62] H. Ohshima, Donnan potential and surface potential of a spherical soft particle in an electrolyte solution, J. Colloid Interface Sci. 323 (2008) 92-97.
[63] K. Makino, H. Ohshima, Soft particle analysis of electrokinetics of biological cells and their model systems, Sci. Technol. Adv. Mater. 12 (2011), 023001.
[64] H.J. Muhren, P. van der Schoot, Electrostatic theory of the acidity of the solution in the lumina of viruses and virus-like particles, J. Phys. Chem B. 127 (2023) 2160-2168.

718 [65] C.J. Milne, D.G. Kinniburgh, W.H. van Riemsdijk, E. Tipping, Generic NICA-Donnan model parameters
719 for metal-ion binding by humic substances, Environ. Sci. Technol. 37 (2003) 958-971.
720 [66] R.M. Town, H.P. van Leeuwen, J.F.L. Duval, Rigorous physicochemical framework for metal ion binding
721 by aqueous nanoparticulate humic substances: Implications for speciation modeling by the NICA-Donnan
722 and WHAM codes, Environ. Sci. Technol. 53 (2019) 8516-8532.
723 [67] J.P. Pinheiro, E. Rotureau, J.F.L. Duval, Addressing the electrostatic component of protons binding to
724 aquatic nanoparticles beyond the Non-Ideal Competitive Adsorption (NICA)-Donnan level: Theory and
725 application to analysis of proton titration data for humic matter, J. Colloid Interface. Sci. 583 (2021) 642-
726 651.
727 [68] V.V. Tran, D. Park, Y.-Ch. Lee. Hydrogel applications for adsorption of contaminants in water and
728 wastewater treatment, Environ. Sci. Pollut. Res. 25 (2018) 24569-24599.
729